Published in final edited form as:
J Clin Neurophysiol. 2010 December ; 27(6): 406–411. doi:10.1097/WNP.0b013e3181fdf8a1.

Propagation of Epileptiform Activity on a Submillimeter Scale

C. A. Schevon, MD PhD[1], **R. R. Goodman, MD PhD**[2], **G. McKhann Jr, MD PhD**[2], and **R. G. Emerson, MD**[1]

[1]Dept of Neurology, Columbia University, New York, NY

[2]Dept of Neurological Surgery, Columbia University, New York, NY

Abstract

Microseizures are highly focal low-frequency epileptiform-appearing events recorded from the neocortex of epilepsy patients. Because of their tiny, often submillimeter distribution they may be regarded as a high resolution window into the epileptic process, providing an excellent opportunity to study the fine temporal structure of their origin and spread. A 16 mm^2 96 microelectrode array with 400 micron interelectrode spacing was implanted in seven patients undergoing invasive EEG monitoring for medically refractory epilepsy. Seven microdischarge populations were tested for a substantial contribution by volume conduction to the observed waveform amplitudes. Single unit activity was examined for specific evidence of neural activity at multiple sites within the microdischarge fields. We found that microdischarges appear to originate at a highly focal source location, likely within a single cortical macrocolumn, and spread to local and more distant sites via neural propagation.

Keywords

multichannel extracellular recording; epilepsy; intracranial EEG; epileptiform discharges; microseizures

Introduction

The epileptogenic zone, or the minimum volume of cortex that must be resected to control clinical seizures, includes the sites from which interictal epileptiform discharges arise, or the “irritative zone”(Rosenow and Luders, 2001). Resecting the irritative zone is part of usual clinical practice, and it has been shown to improve surgical outcomes in neocortical epilepsy (Alarcon et al., 1997; Bautista et al., 1999). However, we lack a definitive model for how best to address the irritative zone surgically; for example, whether all areas included in the field of an epileptiform discharge need be resected. By studying the mechanisms of the origin and spread of interictal discharges we can uncover specific knowledge of the composition of the irritative zone.

Microseizures and microdischarges are highly focal low-frequency epileptiform-appearing events recorded from the neocortex of epilepsy patients using an intracortical array with high spatial resolution (Schevon et al., 2008; Schevon et al., 2009). Because of their tiny, often submillimeter distribution they may be regarded as a high resolution window into the epileptic process, providing an excellent opportunity to study the fine temporal structure of their origin and spread. We put to the test a long held hypothesis in epilepsy literature: that

Corresponding Author: C. A. Schevon, 710 West 168th Street, New York, NY 10032, 212 305-2121, Fax: 212 305-5445, cas2044@columbia.edu.

low frequency waveforms, such as those that make up epileptiform discharges, are seen simultaneously from a large cortical area relative to their site of origin by electrical conduction of the originating event through the tissue medium, or that discharges arise simultaneously from a large cortical region (Nunez and Srinivasan, 2006). We propose instead that low frequency waveforms can and do arise from highly focal cortical domains, and are seen at distant locations not by means of volume conduction, but via neural propagation.

Methods

Microelectrode array implantation and recording

The microelectrode array (MEA) used in this study is an FDA-approved device (Neuroport™ neural monitoring system, Blackrock Microsystems, Salt Lake City, UT) that has been safely implanted in humans at several institutions (Hochberg et al., 2006; House et al., 2006; Waziri et al., 2009). The array measures 4 mm × 4mm, and contains 96 microelectrodes arranged in a regular 10 × 10 square with no electrodes at the corner positions. The individual microelectrodes were platinum-coated silicon, protruding 1 mm from the array base and were electrically insulated except for the terminal 70 microns. They tapered from 35-75 microns in diameter at the base to 3-5 microns at their recording tips. Electrode impedance at manufacture was 322 +/- 138 kOhm.

The MEA was implanted alongside subdural and depth electrodes into the neocortex of patients with medically intractable focal epilepsy undergoing intracranial EEG (iEEG) recording at the Columbia University Medical Center/New York-Presbyterian Hospital to help identify the epileptogenic zone, i.e. the tissue that must be removed to obtain seizure control. Use of the MEA was limited to patients for whom the presurgical evaluation indicated clear seizure localization to a restricted region, in whom invasive recording was performed to refine the resection boundaries, in order to ensure that the implantation site was included in the area targeted for subsequent surgical treatment. Cases that were considered appropriate included temporal lobe epilepsy, in which the implantation was performed to define the contribution of lateral temporal neocortex and tailor temporal lobectomy, and extratemporal syndromes in which scalp EEG recording indicated a consistent and well-defined interictal and ictal focus limited to a sublobar distribution and confirmed by a neuroimaging study. The study was approved by the Institutional Review Board of the Columbia University Medical Center and informed consent was obtained from each patient prior to the procedure.

The MEA was implanted into flat surfaces of exposed neocortical gyri through the pia mater using a pneumatic insertion technique; for more details see (Waziri et al., 2009). The implant site was selected based on the estimation of the epileptogenic region from presurgical studies, as described above, and selected so as to be included in the subsequent surgical treatment. Lateral temporal sites were chosen to fall within the region to be included in anterolateral temporal lobectomy. Extratemporal implantation sites were selected from regions with prominent interictal epileptiform discharges identified by intraoperative corticography, a standard clinical procedure during subdural electrode implantation at our institution. Potentially eloquent sites such as Broca's area or primary motor cortex were avoided. Following implantation, standard clinical macroelectrode grids were placed. The MEA assembly includes two reference wires; one was placed subdurally near the MEA, the other epidurally. During monitoring, MEA data was made available to the clinical team to assist in the surgical evaluation. Following the monitoring period, with duration determined by clinical needs, the MEA was explanted along with the clinical grids.

MEA signals were sampled at 30 kHz/channel (0.3-7.5 kHz bandpass filtering) with 16-bit precision and a range of +/- 8 mV. The reference signal was selected to optimize recording quality; most often, it was found that best results were obtained with the epidural reference. To monitor recording integrity, electrode impedance testing and visual inspection of sample data was performed after the initial hookup and daily thereafter.

Offline, MEA recorded data were downsampled to 500 Hz/channel after low pass filtering at 125 Hz (4^{th} order Butterworth) to yield high spatial resolution local field potential signals in the frequency range of standard EEG ("μEEG"). The μEEG was viewed in a spatially organized, referential montage using a commercial EEG viewing program (Insight, Persyst Development Corp., Prescott, AZ).

Microdischarge identification

One block of six hours of interictal data, recorded between 24 and 48 hours postoperatively, was reviewed for each patient. Microdischarges were visually identified and classified into different populations based on characteristic field and waveform morphology. Analogous to standard clinical EEG recordings, the criteria for identifying microdischarges were based on those used to identify interictal epileptiform discharges, such as: "standing out" from the background, a complex morphology, and disruption of the background pattern (Niedermeyer and Lopes da Silva, 1999). The first 100 examples of each identified discharge population were selected, if present. Only those populations for which 100 examples were seen in the six hour block were then included for further analysis.

Discharge Fields

To align the discharges temporally, the channel at which the maximum deflection was consistently present (the "primary" channel) was selected by visual inspection and absolute amplitude measurements. The time of the peak in the primary channel at which maximum deflection was seen ("t_{max}") was used as the alignment point.

Single-trial instantaneous amplitude in the 1-50 Hz frequency range was computed using the Hilbert transform for the two-second period centered on the discharge peak (i.e., the induced amplitude). Baseline values were determined from the first 500 msec of the two-second period. Single trial amplitude was then averaged across discharges to determine the sites at which each population significantly exceeded baseline values. All channels with amplitude in the 10 msec window centered on t_{max} greater than five standard deviations over the baseline mean were considered to be included in the discharge population field.

Volume Conduction

The volume conduction hypothesis holds that the appearance of a discharge at a given location occurs by omnidirectional transmission of voltage from the source through the intervening tissue (Ruch et al., 1965). Thus,

$$V_{local}=V_d+V_{vc}+V_{\varepsilon}$$

where V_{local} = observed signal amplitude, V_d = discharge amplitude attributed to field potentials generated locally to the recording site, V_{vc} = volume conducted signal amplitude from the discharge source, and V_ε = amplitude of unrelated local activity. According to Coulomb's law, which describes the physics of electrical field strength (Ruch et al., 1965; Zaveri et al., 2009), the volume of the conducted signal amplitude decreases in proportion to the inverse square of the distance from the source, i.e.:

$$V_{vc}=V_{source} * k/x^2 \quad (1)$$

where k is a constant that includes tissue impedance and fixed constants, and x = distance to the source.

The maximum amplitude that could be explained by volume conduction, or V_{vc}, was empirically determined by calculating the minimum signal amplitude as a percentage of the amplitude at the primary channel at a given distance. Each discharge was normalized so that the amplitude at the primary channel was exactly + or -100 uV. The Euclidean distance of each channel to the primary channel was calculated, and the minimum amplitude value at each distance value was determined for the set of 100 discharges in each population.

To address the question of whether the observed discharge field could be explained by synaptic transmission, we tested the hypothesis that temporal differences among channels are due to consistent propagation patterns rather than the result of uncorrelated neural activity. The sample at which the peak occurred was determined by taking the first and second derivatives, and determining the point closest in time to t_{max} at which the first derivative was zero and the second derivative was either positive or negative, depending on whether the maximal amplitude change in that discharge population was negative or positive. Differences in the peak timings at each channel in the discharge field compared to the primary channel were assessed for significance using one-way ANOVA, with Bonferroni correction for multiple comparisons.

Unit Activity

Single neuron firing was detected using spike sorting software from Blackrock Microsystems, Inc (Hochberg et al., 2006; Suner et al., 2005). Single neuron detections were identified from 2 ms windows, then clustered according to waveshape. In this way, more than one distinct unit can be identified from a single channel. At least 5 sample action potential waveforms (if available) were reviewed from each detected unit type to exclude artifactual detections. The total single neuron firing activity temporally associated with microdischarges was determined by summing all detections per unit within a 1 second window centered on t_{max}.

Results

Seven patients were implanted with the MEA and chronically recorded, for periods of up to 4 weeks. Microdischarges with distinct and consistent waveshapes and spatial fields (Figure 1) were recorded from the interictal records of 5 of 7 patients, with up to six distinct populations recognized per patient (Schevon et al., 2008). Of these, there were seven microdischarge populations, recorded from Patients 2, 3, and 4, in which at least 100 examples were found in the 6 hour period reviewed (Figure 2). Discharge populations were labeled according to patient number, with distinct populations from the same patient designated by a letter.

The number of channels meeting criteria for inclusion in each discharge field ranged between one and 11, including the primary channel. The total area covered by each discharge field, then, ranged from 400 × 400 microns or 0.16 sq mm, to 1.76 sq mm, not including space between non-contiguous field channels.

Inspecting the waveforms of a typical microdischarge revealed abrupt amplitude differences between channels inside and outside the field (Figure 3a). In order to measure the degree to

which amplitude varied by distance from the primary channel, the lower envelope of amplitude vs. distance was calculated for all of the microdischarges included in the study sample, after normalizing each so that the primary channel amplitude at t_{max} was fixed at 100 (Figure 3b). These values appeared to be uniformly distributed. In particular, values near zero were found even in the nearest channels.

Differences in the timing of maximum amplitude peak were observed by superimposing the waveforms recorded during individual microdischarges (Figure 2, Figure 3a). To determine whether these timing differences were due to consistent propagation patterns as opposed to uncorrelated neural activity, channels in which the means of the maximum amplitude peaks were significantly different from that of the primary channel (one-way ANOVA with Bonferroni correction, $p < 0.001$) were identified. There were six discharge populations with at least one channel outside the primary channel meeting criteria for inclusion in the microdischarge field (Figure 3c).

The speed of microdischarge propagation was estimated from the average delays of the discharge peaks between channels. Figure 4A shows the average delay of the maximum peak relative to the primary channel for each discharge population, plotted against channel distance in mm. The presence of non-contiguous discharge fields makes using Euclidean distance to calculate propagation speeds somewhat suspect. Indeed, speed estimates showed means ranging between 100 mm/sec and 5 m/s (Figure 4B).

Single neuron detections were aligned in the same way as the low frequency waveforms (Figure 2). Inspection of the raster plots reveal that increased unit activity precedes the discharge peak, during the rising edge of the discharge, in the primary channel for populations 2, 3A, 4A, and 4B (red raster plots). Additionally, increased unit activity with variation in timing that cannot be attributed to the presumed source location was seen in other channels within the discharge field in populations 3A and 4B (black raster plots).

Discussion

Volume conduction is commonly cited to explain the observed fields of epileptiform discharges (Dominguez et al., 2005; Lachaux et al., 2003; Nunez and Srinivasan, 2006). While this is a useful concept when applied to recordings from the scalp, where sensors are placed at considerable distance from the sources of neuroelectric activity, it cannot serve as a significant factor in intracranially recorded EEG (Zaveri et al., 2009). This is due to the rapid decrease in conducted amplitude with distance, which follows an inverse-square law. Additionally, evidence for neural propagation of EEG waveforms has been compiled from scalp EEG recordings of interictal epileptiform discharges (Alarcon et al., 1997; Emerson et al., 1995) and slow oscillations during sleep (Massimini et al., 2004).

Focal paroxysmal low frequency events, which we term “microdischarges”, have been identified in epileptic brain areas using intracortical electrodes (Schevon et al., 2008; Schevon et al., 2009). While the role that these events may play as an epileptic biomarker is still under investigation, the choice of spatial resolution, ideally submillimeter, is important to their detection. Further, we have compiled evidence that volume conduction cannot explain the presence of microdischarges at multiple channels simultaneously. Rather, they appear to originate at a highly focal source location, likely within a single cortical macrocolumn, and spread to local and more distant sites via neural propagation.

Because of the pneumatic implantation method, the MEA is by necessity always placed into a flat, well-visualized cortical surface free of visible blood vessels or structural irregularities. Tissue impedance in the 4mm × 4mm area covered by the MEA is therefore unlikely to vary significantly. Thus, if volume conduction occurs to a significant degree within the area

sampled by the MEA, the geometry of the resulting field should appear symmetric. To the contrary, however, discharge fields of the studied populations showed clear directional bias (eg populations 3A, 4A) and in some cases (populations 2 and 4C) the field was non-contiguous. This effect was seen in both the raw μEEG traces (Figure 1) and in the averaged induced amplitude upon which field determination was based (Figures 1 and 2).

The volume conduction hypothesis was directly tested by measuring waveform amplitude as a function of distance from the primary channel. As electrical conduction through material with similar density to water should occur with no discernable delay, measuring amplitude differences at one recording sample would be expected to demonstrate gradual decreases in waveform amplitude with increasing distance from the source. A counterexample to this hypothesis is revealed in the waveforms for a single discharge from population 4A (Figure 3a). There is a clear separation between the peak amplitude channels inside the discharge field (shown as red traces) and the rest (shown in black). Amplitude changes across each discharge population were also assessed by calculating the lower envelope, or the minimum amplitude present at all channels at a given distance at the exact moment of a discharge peak. This, in turn, represents the *maximum* amplitude that can be attributed to volume conduction. If volume conduction were responsible for a portion of the observed waveform amplitude, the lower envelope would *always* be greater than zero, and the highest values would be closest to the source. We found, however, that the lower amplitude envelope shows values near zero even at close distances, and that the distribution appeared to be uniform with respect to distance (Figure 3b).

Direct support for local neural propagation was obtained by examining the timing of the maximum discharge peak in each channel. While limited temporal resolution may have hampered previous investigations (Wennberg and Lozano, 2003), the recording system used in this study permits the detection of sub-millisecond delays. Statistically significant differences in peak timing compared to that of the primary channel were found (Figure 3c), inconsistent with the notion that any variations could be attributed to uncorrelated neural activity. Additionally, single unit activity increased just prior to the discharge peak in more than one channel in two populations (3A and 4B; Figure 2). This supports the notion that local neuronal activity contributes to the discharge peak.

The finding of non-contiguous microdischarge fields in two of populations (Figure 2), together with the great variation in estimated propagation speeds (Figure 4), suggest that the architecture of the neural pathways subserving the observed waveform propagation is not closely tied to Euclidean distance over the short distances covered by the MEA. This stands in contrast with observations of evoked and spontaneous traveling waves across the surface of rat visual cortex using voltage-sensitive dye imaging (Xu et al., 2007). One explanation is the presence of an “iceberg” effect, in which a larger activity field is present in higher cortical layers, with visibility limited to a small portion of the field in the layers (4 and 5) sampled by the MEA. In particular, the upper layers (1 - 3) are well known to subserve horizontal cortico-cortical connections (Shipp, 2007). Such a view has been proposed as a mechanism for the origin of epileptiform discharges, with an early source in layer 5 followed by horizontal propagation through the superficial layers (Ulbert et al., 2004). Alternatively, local cortical architecture may be remodeled by the process of epileptogenesis or by repeated seizures, with new or strengthened synaptic connections (Schwartzkroin and Knowles, 1984) that serve to speed up the development and propagation of interictal discharges and seizures.

Acknowledgments

Funding for this work was provided by the National Institute of Neurological Disorders and Stroke (K08 NS48871, CAS).

References

Alarcon G, Garcia Seoane JJ, Binnie CD, Martin Miguel MC, Juler J, Polkey CE, et al. Origin and propagation of interictal discharges in the acute electrocorticogram. Implications for pathophysiology and surgical treatment of temporal lobe epilepsy. Brain 1997;120:2259–2282. [PubMed: 9448581]

Bautista RE, Cobbs MA, Spencer DD, Spencer SS. Prediction of surgical outcome by interictal epileptiform abnormalities during intracranial EEG monitoring in patients with extrahippocampal seizures. Epilepsia 1999;40:880–90. [PubMed: 10403211]

Dominguez LG, Wennberg R, Gaetz W, Cheyne D, Snead OC, Velazquez JL. Enhanced synchrony in epileptiform activity? Local versus distant phase synchronization in generalized seizures. Journal of Neuroscience 2005;25:8077–84. [PubMed: 16135765]

Emerson RG, Turner CA, Pedley TA, Walczak TS, Forgione M. Propagation Patterns of Temporal Spikes. Electroencephalography and Clinical Neurophysiology 1995;94:338–348. [PubMed: 7774520]

Hochberg LR, Serruya MD, Friehs GM, Mukand JA, Saleh M, Caplan AH, et al. Neuronal ensemble control of prosthetic devices by a human with tetraplegia. Nature 2006;442:164–171. [PubMed: 16838014]

House PA, MacDonald JD, Tresco PA, Normann RA. Acute microelectrode array implantation into human neocortex: preliminary technique and histological considerations. Neurosurgical FOCUS 2006;20:1–4.

Lachaux JP, Rudrauf D, Kahane P. Intracranial EEG and human brain mapping. Journal of Physiology-Paris 2003;97:613–628.

Massimini M, Huber R, Ferrarelli F, Hill S, Tononi G. The Sleep Slow Oscillation as a Traveling Wave 2004;24:6862–6870.

Niedermeyer, E.; Lopes da Silva, F. Electroencephalography: basic principles, clinical applications, and related fields. Baltimore, MD: Lippincott Williams & Wilkins; 1999.

Nunez, PL.; Srinivasan, R. Electric fields of the brain: the neurophysics of EEG. Oxford; Oxford University Press; 2006.

Rosenow F, Luders H. Presurgical evaluation of epilepsy. Brain 2001;124:1683–700. [PubMed: 11522572]

Ruch, TC.; Patton, HD.; Woodbury, JW.; Towe, AL., editors. Neurophysiology. W. B. Saunders Company; 1965.

Schevon CA, Ng SK, Cappell J, Goodman RR, McKhann G, Waziri A, et al. Microphysiology of Epileptiform Activity in Human Neocortex. Journal of Clinical Neurophysiology 2008;25:321–330. [PubMed: 18997628]

Schevon CA, Trevelyan AJ, Schroeder CE, Goodman RR, McKhann G Jr, Emerson RG. Spatial characterization of interictal high frequency oscillations in epileptic neocortex. Brain 2009;132:3047–3059. [PubMed: 19745024]

Schwartzkroin PA, Knowles WD. Intracellular study of human epileptic cortex: in vitro maintenance of epileptiform activity? Science 1984;223:709–12. [PubMed: 6695179]

Shipp S. Structure and function of the cerebral cortex. Current Biology 2007;17:R443–R449. [PubMed: 17580069]

Suner S, Fellows MR, Vargas-Irwin C, Nakata GK, Donoghue JP. Reliability of signals from a chronically implanted, silicon-based electrode array in non-human primate primary motor cortex. IEEE Trans Neural Syst Rehabil Eng 2005;13:524–41. [PubMed: 16425835]

Ulbert I, Heit G, Madsen J, Karmos G, Halgren E. Laminar analysis of human neocortical interictal spike generation and propagation: current source density and multiunit analysis in vivo. Epilepsia 2004;45 4:48–56. [PubMed: 15281959]

Waziri A, Schevon CA, Cappell J, Emerson RG, McKhann GM 2nd, Goodman RR. Initial surgical experience with a dense cortical microarray in epileptic patients undergoing craniotomy for subdural electrode implantation. Neurosurgery 2009;64:540–5. discussion 545. [PubMed: 19240617]

Wennberg RA, Lozano AM. Intracranial volume conduction of cortical spikes and sleep potentials recorded with deep brain stimulating electrodes. Clinical Neurophysiology 2003;114:1403–1418. [PubMed: 12888022]

Xu W, Huang X, Takagaki K, Wu Jy. Compression and Reflection of Visually Evoked Cortical Waves. Neuron 2007;55:119–129. [PubMed: 17610821]

Zaveri HP, Duckrow RB, Spencer SS. Concerning the observation of an electrical potential at a distance from an intracranial electrode contact. Clinical Neurophysiology 2009;120:1873–1875. [PubMed: 19748311]

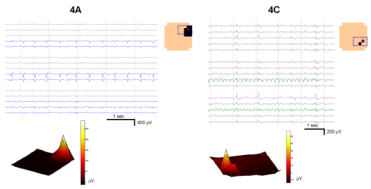

Figure 1. Microdischarge fields recorded by the MEA

Two populations from Patient 4 (4A and 4C) are shown, displaying stereotyped but distinctive location, fields, and waveshape. The μEEG in a subset of the MEA, shown in the channel layout schematic in the upper right enclosed in a dotted blue box, is displayed. Channels within the discharge field are indicated by colored traces. Averaged instantaneous amplitude of all 100 discharges in each population at the time of the reference channel peak (t_{max}) is shown on the physical MEA layout (color spectrum plots, bottom). Channels meeting criteria for inclusion in the field are shown in the layout schematic as solid squares, with the red square denoting the primary channel. In both the averaged and the individual waveform views, there is an abrupt transition between channels within and outside of the discharge field that does not follow a symmetric spatial pattern. In particular, the population in 4C is maximal in channels that are not immediately adjacent.

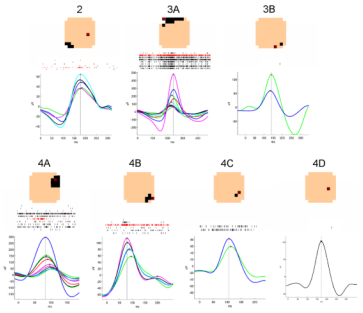

Figure 2. Summary of the seven microdischarge populations

A typical microdischarge from each population is shown, with each μEEG trace representing one channel in the discharge field. Waveforms in which the maximum deflection was negative are shown inverted. The timing of the peak value in each channel is shown marked with an asterisk; a vertical line is drawn through the peak in the reference channel, indicating the time used for alignment of the selected discharges. A raster plot of single neuron detections from all the discharges included in each sample is displayed above the EEG traces. At the top are layout schematics showing the field of each population, as in Figure 1. The primary channel is shown in red in both the layout schematic and the raster plots.

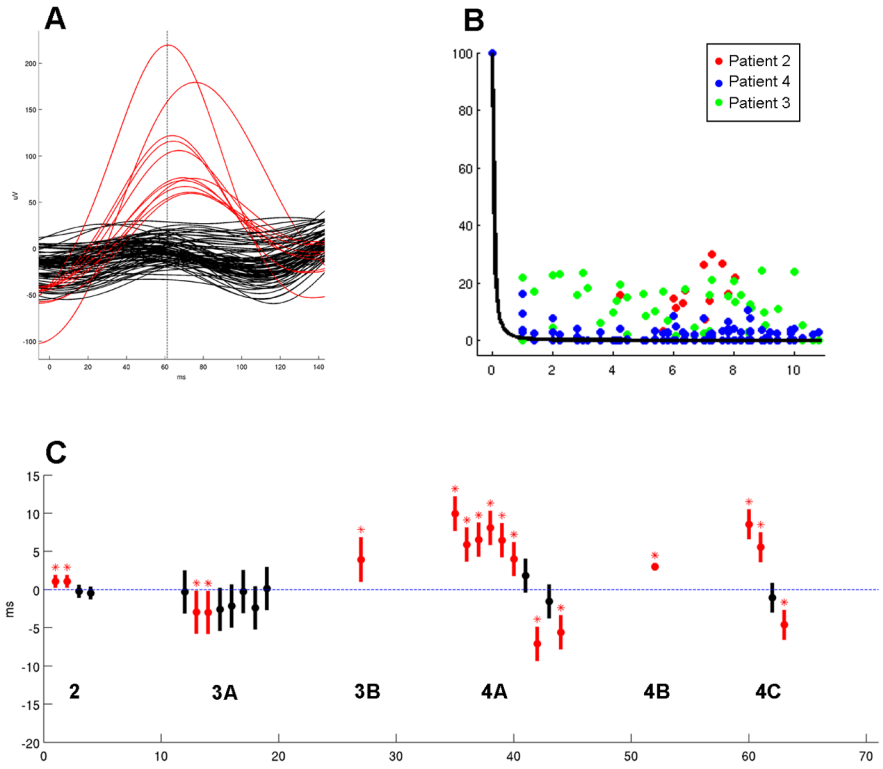

Figure 3. Evidence against the volume conduction hypothesis for dense intracortical recordings

A) Simultaneous μEEG traces during a single microdischarge from Patient 4, with channels within the discharge field shown in red and the remaining channels in black. Note the lack of an even gradation of voltage that would be expected if waveform amplitude is continuously dependent on distance from the discharge source. B) Amplitude lower envelope, color coded according to patient, showing a uniform distribution with respect to distance. No significant difference in means was found between the channels nearest to the source (<= 3) and those farthest away (>= 9) (one-way ANOVA, alpha of 0.05). Superimposed on these is a 1/xˆ2 curve (Equation 1), which best explains the observed values and illustrates the steep drop-off of 1/xˆ2. C) Averaged peak timing of each field channel relative to the primary channel, arranged by population. Negative values indicate that the peaks in these channels preceded that of the primary channel, and positive values indicate a lag. Mean peak delays are indicated by the solid circles, and standard deviation by the vertical bars. Mean values that are significantly different from zero (blue dotted line) are shown in red and marked with an asterisk (one-way ANOVA with Bonferroni correction, $p < 0.001$).

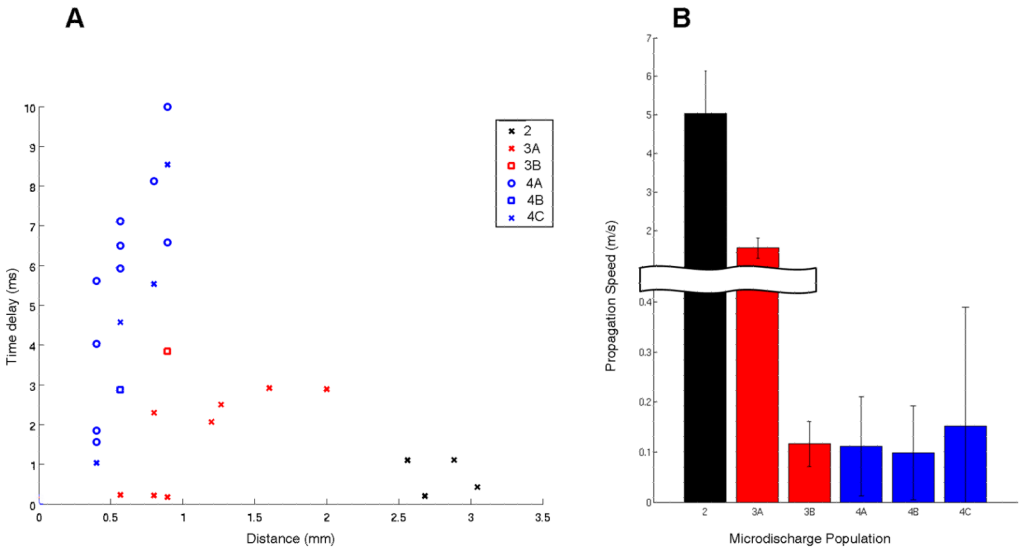

Figure 4. Estimation of propagation speed

A) Absolute values of the average peak time lead or lag per channel in each microdischarge field is plotted against the distance from the primary channel, with color and symbol used to code for patient and discharge population. B) Bar plot showing the mean and standard deviation of propagation speeds in meters per second, calculated for each population. Mean speeds ranged from 100 mm/sec (population 4B) to 5 m/sec (population 2). The observed variation suggests that local propagation speed is highly dependent on the structure of the underlying neural architecture.